Chinese Physics Letters

LETTER

Interaction Between Yin-Yang Vortex States and Topological Edge States in UTe_2

Cite as: Yuguang Wang *et al*. 2026 *Chin. Phys. Lett.* **43** 110712

DOI CSTR

Recommended Articles

Hybrid Skin-Topological Effect Induced by Eight-Site Cells and Arbitrary Adjustment of the Localization of Topological Edge States
Jianzhi Chen, Aoqian Shi, Yuchen Peng, Peng Peng, and Jianjun Liu
Chin. Phys. Lett. **41**, (2024)

Observation of Zero-Energy Modes with Possible Time-Reversal Symmetry Breaking on Step Edge of $CaKFe_4As_4$
Lu Cao *et al*.
Chin. Phys. Lett. **41**, 117401 (2024)

Observation of Robust In-Gap Edge States in $EuRbFe_4As_4$
Xu-Hui Ning *et al*.
Chin. Phys. Lett. , (2026)

Anisotropic Strain at Atomic Steps in SnTe(111)/Au(111) Heterostructures Revealed by Moiré Superlattices
Rui-Qi Cao, Jeison Fischer, Dirk Sander, Stuart S. P. Parkin, and Kai Chang
Chin. Phys. Lett. **43**, 060714 (2026)

Coexisting Commensurate Pair Density Waves in 6R-TaS_2
Hongqin Xiao, Yuxuan He, Ke Zhu, Yuhan Ye, Yumeng Li, Lijing Huang, Pucen Xiong, Haitao Yang, Geng Li, and Hong-Jun Gao
Chin. Phys. Lett. **43**, 060713 (2026)

Atomic Visualization of Bulk and Surface Superconductivity in Weyl Semimetal γ-$PtBi_2$
Hao Zhang *et al*.
Chin. Phys. Lett. **42**, 120708 (2025)

A series journal of Chinese Physical Society distributed by IOP Publishing

Chinese Physics Letters

Chin. Phys. Lett. **43** 110712 (2026)

LETTER

DOI: 10.1088/0256-307X/43/11/110712
CSTR: 32039.14.0256-307X.43.11.110712

Interaction Between Yin-Yang Vortex States and Topological Edge States in UTe_2

Yuguang Wang(王宇光)[1,2,†], Yuanji Li(李元骥)[1,2,†], Dengpeng Yuan(袁登鹏)[3,†], Ruotong Yin(尹若彤)[1], Jiashuo Gong(巩佳硕)[1,2], Jiakang Zhang(张嘉康)[1], Shiyuan Wang(王适源)[1], Weiyi Liu(刘唯一)[3], Shiyong Tan(谭世勇)[3,*], Dong-Lai Feng(封东来)[2,*], and Ya-Jun Yan(闫亚军)[1,2,*]

[1]Hefei National Research Center for Physical Sciences at the Microscale, University of Science and Technology of China, Hefei 230026, China
[2]New Cornerstone Science Laboratory, Hefei National Laboratory, Hefei 230088, China
[3]National Key Laboratory of Surface Physics and Chemistry, Mianyang 621908, China

[†]These authors contributed equally to this work.
[*]Corresponding authors. Email: sytan4444@163.com; dlfeng@hfnl.cn; yanyj87@ustc.edu.cn

UTe_2, a strong candidate for spin-triplet superconductivity, hosts novel step-edge states and Yin-Yang vortices on its (011) surface, both of which are intimately connected to topological surface states. However, the interaction between these two types of states remains unexplored. Here, we use scanning tunneling microscopy/spectroscopy (STM/STS) to investigate the coupling between step-edge states and Yin-Yang vortex states in UTe_2. We uncover pronounced edge–vortex interactions, and find that the resulting in-gap spectral reconstruction is spatially asymmetric and depends sensitively on the position of the step edge relative to the vortex. Most strikingly, when the Yang vortex directly coincides with the step edge, the zero-energy conductance peak, a candidate Majorana mode signal, is locally suppressed. Our findings reveal an unexplored interplay between topological boundary states and vortex bound states in a spin-triplet superconductor and establish step edges as a local tuning factor for vortex zero modes, providing possibilities for spatially selective manipulation of candidate Majorana modes through engineered boundary geometries.

Introduction

Spin-triplet superconductors feature Cooper pairs formed by spin-parallel electrons [1,2]. This distinct pairing mechanism gives rise to a host of exotic properties far beyond those of spin-singlet superconductors, including large upper critical fields far exceeding the Pauli limit [3–5], magnetic-field-induced superconducting reentrance [4,6], topological surface/edge states [7–9], and half-quantized vortices [10,11]. More importantly, spin-triplet superconductors might be promising platforms for topological superconductivity and Majorana quasiparticles [7,12–15]. They have thus attracted broad interest in condensed matter physics and quantum information science.

In recent years, UTe_2 has emerged as a strong candidate for spin-triplet superconductivity [16–28]. The supporting evidence includes weak temperature dependence of the Knight shift across the superconducting transition [18,29–32], large upper critical fields exceeding the Pauli limit in all crystallographic directions [16,17,33], magnetic-field-induced superconducting reentrance [34–38], etc. Furthermore, scanning tunneling microscopy/spectroscopy (STM/STS) studies have uncovered novel boundary and vortex states on the UTe_2 (011) surface [21,39–41]. On the one hand, step edges on this surface exhibit pronounced in-gap states closely related to superconductivity, with particle–hole asymmetry: for steps facing the [0−1−1] direction, the edge states show a peak at negative energy and a suppression of local density of states (LDOS) at positive energy; the opposite behavior is observed for steps facing the [011] direction [21,41]. These complementary features were initially interpreted as signatures of chiral edge states associated with chiral spin-triplet superconductivity with time-reversal symmetry breaking (TRSB) [21]. However, more recent Kerr effect and muon spin relaxation (μSR) measurements on high-quality UTe_2 samples have reported no evidence of TRSB [42,43], challenging the early interpretation of chiral superconductivity/edge states. On the other hand, under perpendicular magnetic fields, anisotropic single-flux-quantum vortices have been observed, exhibiting a distinctive bright–dark contrast [39–41]. The bright part displays a sharp zero-energy conductance peak (ZECP), while the dark part shows sharper superconducting gap features. Our theoretical analysis suggests that this vortex pattern arises from the asymmetric suppression of topological surface states (TSS) by the vortex on the tilted (011) surface [39]. Remarkably, the ZECP in the bright part of the vortex has a full width at half maximum of only 0.2 meV and remains unsplit over a spatial range of tens of nanometers and under magnetic fields up to 8 T, making this vortex state a strong candidate for Majorana zero modes (MZMs) [39,40].

Given that both the step-edge states and the vortex states described above are intimately associated with spin-triplet superconductivity, a fundamental question arises: how do these two distinct types of states interact when brought into spatial proximity? In this work, we use STM/STS to address this question and find a clear coupling effect between the two types of states that depends strongly on their relative position. Most strikingly, when the bright vortex part directly overlaps with the step edge, the ZECP inside the vortex is locally suppressed, demonstrating that step edges can serve as an effective way to tune vortex zero modes.

Methods

Synthesis of UTe_2 Single Crystals

High-quality UTe_2 single crystals were synthesized via the molten salt flux (MSF) technique employing an equimolar NaCl-KCl mixture (99.99% purity, Alfa Aesar) as a flux. Uranium metal pieces (mass < 0.4 g) were initially etched in nitric acid to eliminate surface oxides. Under an argon atmosphere in a glovebox, tellurium pieces (Te, 99.999% purity, Alfa Aesar) were combined with uranium at a U:Te molar ratio of 1:1.65, along with NaCl-KCl flux at a U:salt molar ratio of 1:60. The reactants were loaded into a carbon crucible

Received 14 September 2026; accepted 20 October 2026; published 30 October 2026
© 2026 Chinese Physical Society and IOP Publishing Ltd. All rights, including for text and data mining, AI training, and similar technologies, are reserved.

Check for updates

lined with quartz wool to prevent material loss during heating. Then the crucible was placed in a quartz tube and heated to 180 ℃ under high vacuum (< 5×10^{-4} Pa) for dehydration. Subsequently, the ampoule was vacuum-sealed and placed in a box furnace, where the mixture was heated to 950 ℃ over 24 hours and maintained at this temperature for 48 hours. It was then cooled gradually at a rate of 0.03 ℃/min to 650 ℃, held at this temperature for 48 hours, and finally cooled to ambient temperature naturally. After the growth process, the ampoules and crucibles were mechanically cleaved, and bulk UTe_2 crystals were manually collected and stored under an argon atmosphere to prevent oxidation.

STM Measurements

UTe_2 crystals were mechanically cleaved at 80 K in ultrahigh vacuum with a base pressure below 2×10^{-10} mbar and immediately transferred into a UNISOKU-1600 STM. Pt-Ir tips were used for STM measurements after being treated on a clean Au (111) substrate. The dI/dV spectra were collected by a standard lock-in technique with a modulation frequency of 973 Hz and a modulation amplitude ΔV of 30–80 μV. The data in the main text were collected at ~ 40 mK with an effective electron temperature $T_{\rm eff}$ of ~170 mK.

Experimental Results

Step-Edge States and Free Yin-Yang Vortices on UTe_2 (011) Surface

Figure 1(a) shows a typical topographic image of two opposite step edges on the UTe_2 (011) surface. The height profile in the lower panel reveals a step height of ~5.6 Å on both sides, corresponding to a single-unit-cell step [21]. The inset displays the projected crystal structure of this plane, showing that U and Te atomic chains run along the crystallographic a-axis, while the stacking sequence breaks the mirror symmetry along the perpendicular direction, i.e., the b^*-axis. This structural asymmetry gives rise to distinct atomic configurations at the two step edges, which we define as the left and right step edges for convenience. The representative dI/dV spectra collected on the two step edges (the L and R points) are displayed in Fig. 1(b), with the spectrum at a reference position away from step edges (the M point) listed as well. The spectrum at M exhibits an obvious superconducting gap, while those at the left and right step edges show pronounced in-gap states peaked at $E_- = -0.12$ meV and $E_+ = 0.12$ meV, respectively, consistent with previous STM studies [21].

Figures 1(c)–1(f) present representative dI/dV maps acquired around the left and right step edges at energies E_+ and E_-, respectively, with their topographic images displayed in Supplementary Note 1 of the Supplementary Materials (SM). For the right edge [Figs. 1(c) and 1(d)], the LDOS is enhanced at E_+ and suppressed at E_-, while the left edge exhibits the opposite behavior. These complementary intensity patterns reveal distinct particle–hole-asymmetric spectroscopic responses at the two opposite step edges. The corresponding LDOS profiles [lower panels of Figs. 1(c)–1(f)] reveal that these in-gap states are spatially localized within approximately 2 nm around the step edges. In addition, the spatial distribution of the right step-edge state appears much more uniform than that of the left step-edge, which is likely related to the detailed lattice structure of the respective step edges. In addition, previous STM studies reported that these step-edge features weaken with increasing temperature or magnetic field, becoming difficult to resolve near the superconducting transition temperature or upper critical field [21,41]. All these characteristics support a close connection between the step-edge states and superconductivity, which are probably associated with boundary states of spin-triplet superconductivity. However, we cannot fully exclude the contribution from trivial edge states arising from altered local atomic configurations at the step edges. Distinguishing these possibilities

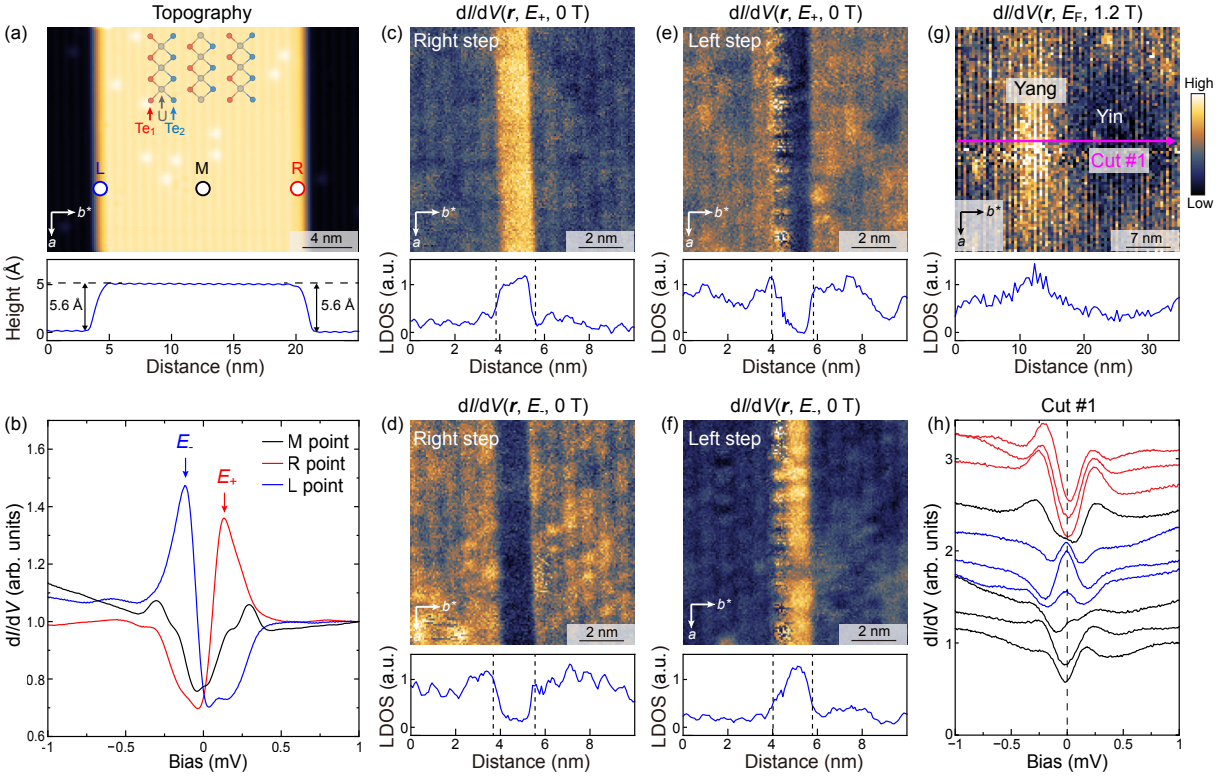

Fig. 1. Step-edge states and free Yin-Yang vortex on UTe_2 (011) surface. (a) Typical topographic image of step edges on UTe_2 (011) surface. The inset shows the projected atomic structure of the UTe_2 (011) surface, and the lower panel displays the height profile of the step edges. (b) Typical dI/dV spectra collected at the L, M, and R points as indicated by the blue, black and red dots in panel (a). (c)–(f) dI/dV maps collected around the right and left step edges at E_+ and E_- energies, respectively. The lower panels show the LDOS profiles across the steps. (g) Zero-energy dI/dV map showing a free Yin-Yang vortex under $B_\perp = 1.2$ T. The lower panel shows the LDOS profile along cut #1 marked in panel (g). (h) dI/dV spectra taken along cut #1, which are vertically shifted for clarity. Measurement conditions: (a) $V_b = 100$ mV, $I_t = 50$ pA; (b) and (h) $V_b = 1$ mV, $I_t = 400$ pA, $\Delta V = 30$–50 μV; (c)–(g) $V_b = 3$ mV, $I_t = 80$ pA, $\Delta V = 60$–80 μV.

requires further theoretical modeling incorporating realistic step-edge structures and the superconducting pairing symmetry of UTe_2.

Figure 1(g) shows a zero-energy dI/dV map acquired under $B_\perp$ = 1.2 T, revealing a characteristic free Yin-Yang vortex located away from step edges. The vortex is termed "Yin-Yang" owing to its contrasting dark-bright pattern, which resembles the conjugate structure of Yin-Yang diagram in Taoism. The LDOS contrast between the Yin and Yang parts is further illustrated by the spatial profile across the vortex [lower panel of Fig. 1(g)], from which the vortex size is estimated to be approximately 25 nm. Figure 1(h) displays the dI/dV spectra taken across the vortex along cut #1 marked in Fig. 1(g). Traversing from the outside through the vortex, the spectrum evolves from a superconducting gap (black curves) to a ZECP at the Yang part (blue curves), and then to an enhanced superconducting gap with increased gap depth at the Yin part (red curves). These findings agree with earlier reports [39–41], and establish a reliable baseline for investigating the interaction between the step-edge states and vortex states.

Position-Dependent Coupling Between Step-Edge States and Yin-Yang Vortex States

We next investigate the coupling between the step-edge states and Yin-Yang vortex states. Notably, the markedly different spatial extents of the two types of states, together with the internal Yin-Yang configuration of the vortex, enable the study of position-dependent coupling between them.

Taking the right step as an example, figure 2(a) presents a zero-energy dI/dV map acquired at $B_\perp$ = 1.2 T for a region containing three successive right steps, revealing several Yin-Yang vortices near the step edges. To quantify the spatial relationship between the step edge and the vortex, we define the distance d from a right step edge (white dashed lines) to the center of the Yang vortex immediately to its left, as illustrated in Fig. 2(a). The determination of d and its uncertainty is described in Supplementary Note 2 of SM. As d increases, the step edge gradually moves away from the Yang vortex center toward the Yin vortex, eventually crossing the Yin vortex and entering the vortex-free region. Multiple cases with distinct d values can be identified from Fig. 2(a).

Figure 2(b) presents the dI/dV map at E_+ = 0.12 meV, revealing that the step-edge state is locally modified by nearby vortices, as highlighted by the cyan dashed boxes. This interaction is further corroborated by the spectra shown in Fig. 2(c). Under $B_\perp$ = 1.2 T, the spectra measured at the vortex-modulated positions [points A–C in Fig. 2(b)] exhibit a pronounced redistribution of in-gap states compared with the zero-field spectrum at the right step edge. Moreover, the spectral line shape varies systematically with the distance d; specifically, the spectra at smaller d show a greater departure from the zero-field reference.

To further elucidate the step-edge–vortex coupling at different distances d, figures 2(d)–2(i) present the spatial evolution of dI/dV spectra across the vortex along the a-axis for three representative cases [cuts #2–#4 in Fig. 2(a)]. The gray and red dashed lines mark E_F and the zero-field E_+ positions, respectively. For d = 13.2 nm and 21.9 nm, where the step edge lies within the Yin vortex region, the spectral modification mainly manifests as a shift of the E_+ peak toward more positive energy, accompanied by the emergence of a weak negative-energy peak. For d = 4.8 nm, where the step edge is in close proximity to the Yang vortex, a splitting-like evolution becomes more apparent: the spectral weight is redistributed such that one component shifts toward E_F, while another emerges at more positive energies, alongside a feature on the negative-energy side. The spectra in the lower panels of Figs. 2(d)–2(f) were acquired from positions equivalent to the C, B, and A points, respectively, but on a reference free vortex away from step edges. It is evident that, in the presence of the step edge, the spectra deviate significantly from the characteristic spectrum in free vortex at the equivalent positions.

A series of control experiments were performed to clarify the respective contributions of the magnetic field, the vortex arrangement, and the step–vortex distance d to the observed spectral changes. Firstly, when the vortex is sufficiently far from the step edge, applying different magnetic fields mainly reduces the intensity of the E_+ peak without producing the systematic peak shifts and spectral-weight redistribution described above, as demonstrated in Supplementary Note 3 of SM and reported previously in Refs. [21,41]. This indicates that the magnetic field alone cannot account for the observed spectral evolution. Secondly, Supplementary Note 4 of SM shows that three high-field cases approximately correspond to the three representative relative step–vortex configurations sampled in Fig. 2 at $B_\perp$=1.2 T, and these cases exhibit qualitatively similar spectral evolution despite the different magnetic fields and vortex arrangement. Thirdly, we have also characterized the behavior of the left step edge, as detailed in Supplementary Note 5 of SM. A similar coupling effect is revealed, which appears as the energy-reversed counterpart of the right step-edge case. These observations collectively demonstrate the coupling between the step-edge states and the vortex states, in which the step–vortex distance d is the dominant parameter governing the systematic spectral evolution, while magnetic field and local vortex arrangement may introduce additional modifications to the peak intensity and peak width.

More importantly, the step-edge–vortex interaction is highly localized, confined to the region where the step-edge state and the vortex spatially overlap. From Figs. 2(a) and 2(b), this confinement range can be estimated to be approximately the vortex size along the a-axis (~10–20 nm) and the spatial extent of the step-edge state along the b^*-axis (~2 nm). This is further supported by Fig. S4 in SM, which presents the evolution of dI/dV spectra across the step edge along the b^*-axis. The spectral modification is observed only in the step-edge region; away from it, the spectra revert to either the pristine superconducting gap structure or the characteristic spectrum in a free vortex.

Suppression of the ZECP in Yang Vortex by the Step-Edge States

A special case, in which the step edge directly overlaps with the Yang vortex, provides an opportunity to examine how the step-edge state modifies the ZECP in the Yang vortex. For comparison, figures 3(a) and 3(b) show a free vortex away from step edges and a vortex whose Yang part coincides with a right step edge.

For the free vortex, the LDOS is strongest at the center of the Yang vortex and decays gradually away from it [left panel of Fig. 3(c) and black curve in Fig. 3(d)]; and a ZECP persists in the Yang vortex, as demonstrated by the dI/dV spectra in Figs. 3(e) and 3(f). In contrast, when the step edge overlaps with the Yang vortex, the zero-energy DOS map clearly reveals a DOS suppression in the step-edge region [middle and right panels of Fig. 3(c)], which is further confirmed by the dips in the corresponding LDOS profiles [red and blue curves in Fig. 3(d)]. Moreover, the dI/dV spectra shown in Figs. 3(g) and 3(h) also reveal pronounced suppression of the ZECP at the step edge. Along cut #8 in Fig. 3(b), taken along the right step edge within the Yang-vortex region, the ZECP is strongly suppressed and the spectra evolve toward the characteristic step-edge-state line shape. Along cut #7, taken across the right step edge along the b^* direction, the ZECP appears away from the edge (black curves), is suppressed right at the step-edge position (blue curves), and reappears after crossing the edge (black curves). Consistent with the observations above, this suppression is also highly localized, confined strictly to the spatial extent of the step-edge states. Figure 3(i) compares the averaged spectra of the data shown in Figs. 3(f) and 3(h), further confirming the striking difference between the free Yang vortex and the Yang vortex influenced by the step edge: in the latter case, the zero-energy DOS is strongly suppressed, and the zero-energy peak can no longer be resolved.

This suppression of the ZECP is surprising; once suppressed, the spectrum resembles the pristine step-edge-state line shape, which naturally raises the question of whether a tunneling-matrix-element effect at the Yang vortex overlapped with the step edge causes the step-edge states to dominate the tunneling. To assess the role of such an effect and to rule out a trivial superposition scenario for the observed

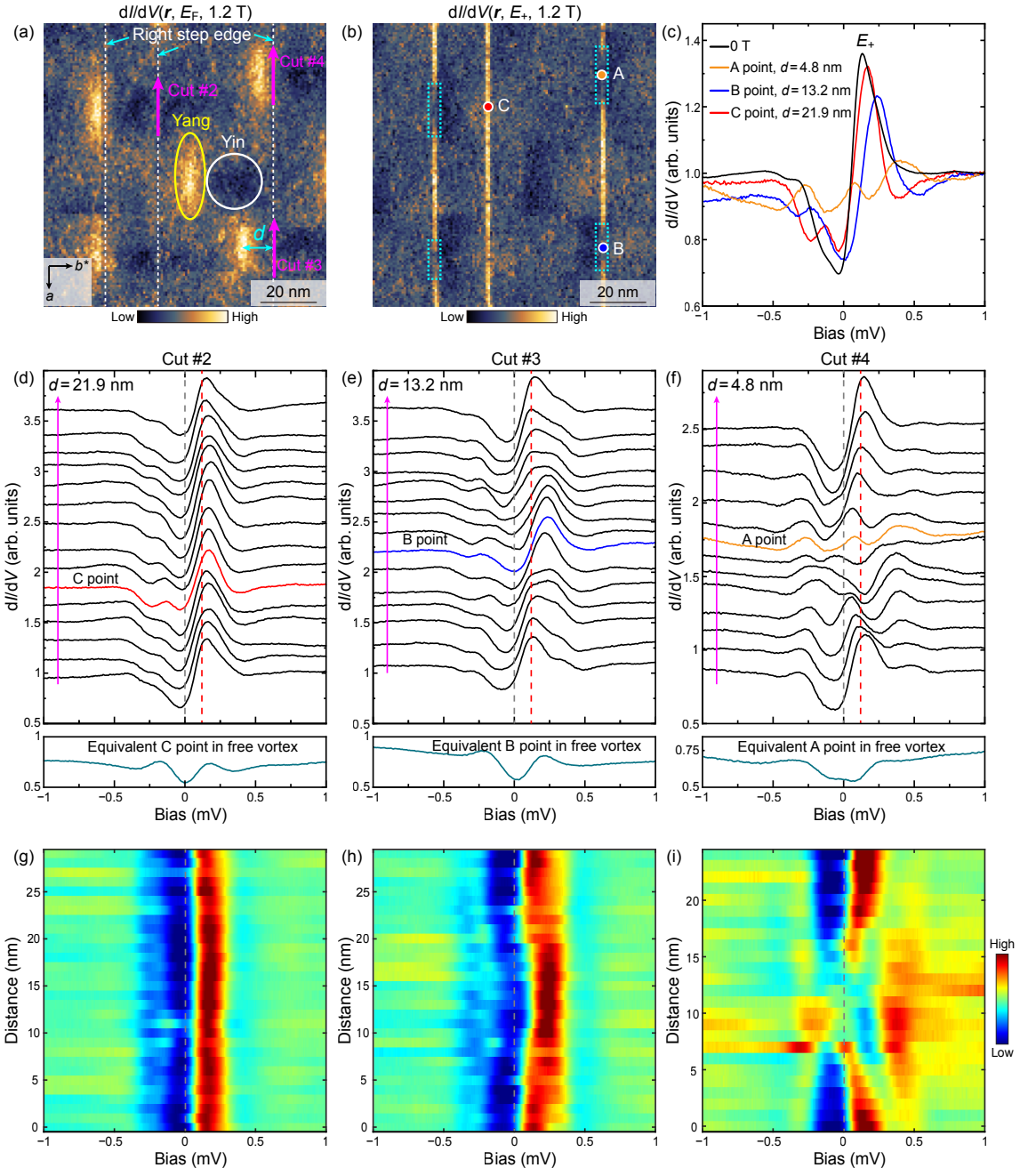

Fig. 2. Interaction between right step-edge states and Yin-Yang vortex states. (a) Zero-energy dI/dV map acquired at $B_\perp$ = 1.2 T for a region containing three successive right steps. The positions of the step edges are marked out by the white dashed lines and cyan arrows. The cyan bidirectional arrow indicates the distance d between a right step edge and a Yang vortex on its left side. (b) dI/dV map at E_+ energy under $B_\perp$ = 1.2 T in the same field of view of panel (a). The cyan dashed boxes show the step-edge regions influenced by vortices. (c) Comparison of dI/dV spectra taken at the right step edge under $B_\perp$ = 0 T and at points A–C at $B_\perp$ =1.2 T. (d)–(f) dI/dV spectra taken along cuts #2–#4 in panel (a), respectively. The lower panels of (d)–(f) show reference spectra acquired at equivalent C, B, and A positions shown in panel (b), respectively, but on a free vortex away from step edges. (g)–(i) Color plots of panels (d)–(f). Measurement conditions: (a) and (b) V_b = 3 mV, I_t = 80 pA, ΔV = 60 μV; (c) V_b = 1 mV, I_t = 200–400 pA, ΔV = 50 μV; (d)–(i) V_b = 1 mV, I_t = 200 pA, ΔV = 50 μV.

spectral changes for all d cases, we perform a simple algebraic summation of the vortex and step-edge spectra with various weighting factors, as detailed in Supplementary Note 6 of SM. Such a simple superposition fails to reproduce the systematic spectral evolution observed in Figs. 2(d)–2(f), 3(g), and 3(h) at different d. Therefore, the observed spectral evolution cannot be explained by a simple algebraic superposition or a tunneling-matrix-element effect, which instead supports an interaction-induced reconstruction of the in-gap spectral weight. Since this interaction should be applicable at all step–vortex distances, the case in which the step edge overlaps with the Yang vortex should not be an exception. We therefore suggest that the local interaction between the step-edge states and the Yang-vortex states also contributes to the observed suppression of the ZECP in the overlap configuration. Besides, we find that when the step edge does not reside on the Yang vortex, the ZECP remains unaffected regardless of the distance d, as shown in Fig. 3(j). Consequently, the step-edge states can locally tune the zero-energy mode inside the Yang vortex.

Spectroscopic Evolution with Step–Vortex Distance

To summarize the evolution of the step-edge–vortex interaction, we compile dI/dV spectra acquired at different magnetic fields and distances d, as displayed in Figs. 4(a) and 4(b). Because the magnetic field changes the vortex size and the vortex separation, and hence the

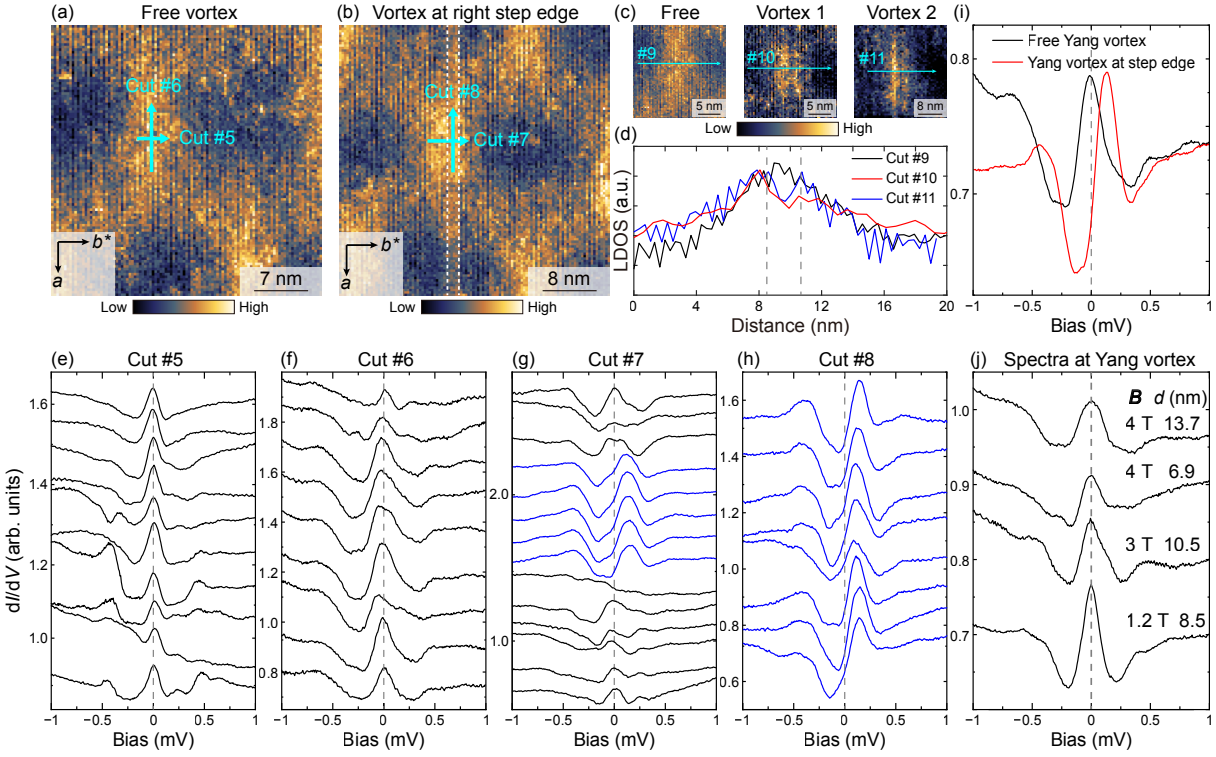

Fig. 3. Comparison between free Yang vortices and Yang vortices at right step edges. (a) and (b) Zero-energy dI/dV maps for a free vortex away from step edge and a vortex with its Yang part overlapped with a right step edge, respectively, measured at $B_\perp$ = 4 T. The white dashed lines mark the position of the right step edge. (c) Enlarged views of the zero-energy dI/dV maps for a free Yang vortex (left panel) and two Yang vortices overlapped with right step edges (middle and right panels). (d) LDOS line profiles taken along cuts #9–11 in panel (c). (e)–(h) dI/dV spectra taken along cuts #5–#8 marked in panels (a) and (b). (i) Comparison of the averaged spectra for the data shown in panels (f) and (h), for a free Yang vortex and a Yang vortex at the step edge, respectively. (j) dI/dV spectra at Yang vortex under $B_\perp$ = 1.2 T–4 T and at different d. Measurement conditions: (a)–(c) V_b = 3 mV, I_t = 80 pA, ΔV = 60 μV; (e)–(j) V_b = 1 mV, I_t = 200 pA, ΔV = 50 μV.

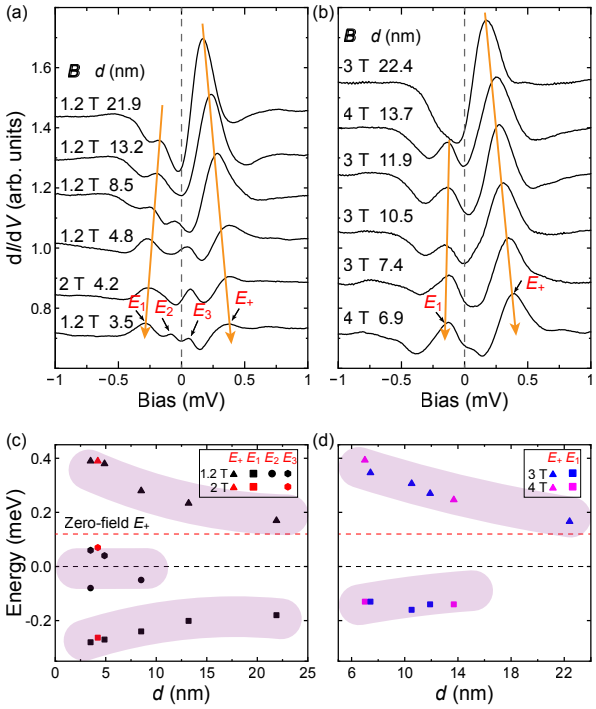

Fig. 4. Spectroscopic evolution as a function of step–vortex distance. (a) and (b) Representative dI/dV spectra at different d under $B_\perp$ = 1.2 T–4 T, which are vertically shifted for clarity. The orange arrows roughly mark out the shift of the spectral peaks. (c) and (d) Extracted energies of all discernible spectral peaks as a function of d. The purple-shaded regions roughly guide the eye to the peak evolution. Measurement conditions: (a) and (b) V_b = 1 mV, I_t = 200 pA, ΔV = 50 μV.

effective value of d at different fields, we show the lower- and higher-field data sets separately to provide a controlled comparison. These spectra reveal a systematic evolution of the in-gap spectral features with decreasing d. The dominant positive-energy peak E_+ shifts progressively toward higher energies, while its spectral weight gradually decreases overall. Concurrently, the spectral weight on the negative-energy side exhibits an opposite trend: it increases gradually and develops into a peak-like structure (E_1) whose position shifts toward lower energies. Furthermore, when d is very small, additional fine spectral structures emerge near E_F, as indicated by the E_2 and E_3 peaks in Fig. 4(a).

The characteristic energies of these discernible peaks were fitted using Gaussian functions with a common constant background for each spectrum, as described in Supplementary Note 7 of SM. The energy evolution of these peaks is quantitatively presented in Figs. 4(c) and 4(d) for the lower- and higher-field conditions, where the purple shaded regions roughly guide the eye. Two features are evident. Firstly, the evolution trends of the spectra under both lower- and higher-field conditions are very similar. Secondly, the spectral evolution is spatially asymmetric, mirroring the asymmetric Yin-Yang vortex structure. When the step edge is located in the Yin-vortex region at medium d values, the spectral variation mainly manifests as peak shifts; in contrast, when the step edge approaches the Yang vortex at smaller d, additional fine spectral structures emerge near E_F.

Discussion and Conclusion

We now discuss the possible origin of these experimental observations. The spectral evolution induced by the step–vortex interaction exhibits a strong position dependence and is closely tied to the Yin-Yang vortex configuration. A natural starting point is therefore to ask whether the same underlying mechanism that produces the

Yin-Yang vortex also acts on the step-edge states, or whether the step-edge states couple directly to the Yin-Yang vortex states.

We first consider a framework similar to that used previously to describe the Yin-Yang vortex configuration on the UTe_2 (011) surface [39]. Our recent work attributed the Yin-Yang vortex configuration to the asymmetric suppression of TSS by the pairing potential around the vortex, driven by the tilted Fermi surface on the (011) surface [39]. In this picture, the bulk vortex preserves mirror symmetry, but on the (011) surface the TSS and vortex bound states remain robust in the Yang vortex, whereas in the Yin vortex the pairing potential drops and/or changes sign, which distorts and extends the TSS wavefunction and leads the suppression of low-energy spectral weight. Since the step-edge states are considered boundary manifestations of these TSS [21,44], the same mechanism may also act on them. Their response should depend on the position of the step edge relative to the vortex, where they experience different local pairing potentials and thus different degrees of wavefunction modification.

We further note that the spectral modification is more pronounced near the Yang vortex and weaker in the Yin vortex, where mainly a shift of the E_+ peak is observed (Fig. 4). This contrast can be understood in terms of the availability of low-energy spectral weight for coupling [45,46]. In the Yin vortex region, the low-energy DOS have already been suppressed, leaving limited spectral weight for the step-edge state to couple to. In contrast, near the Yang vortex, the TSS and vortex bound states remain robust, enabling strong coupling with the step-edge states and leading to a pronounced redistribution of in-gap spectral weight. Combined, these two pictures can account for the asymmetric spatial evolution of low-energy spectral weight and for why the most dramatic spectral reconstruction occurs near the Yang vortex. We also note that these pictures currently remain largely phenomenological; quantitative theoretical modeling incorporating the specific pairing symmetry and surface state dispersion of UTe_2 is still required.

Another common mechanism by which a vortex affects the in-gap spectral weight is the phase/superfluid (Doppler-like) effect [47–49]. However, several observations argue against it being the dominant mechanism here. Firstly, the spectral evolution is spatially asymmetric and depends strongly on the Yin-Yang configuration, rather than solely on the distance to the vortex core. Secondly, the evolution trend is nearly identical at 1.2 T and 4 T, whereas a Doppler-dominated effect would be expected to show field dependence. Thirdly, the observed peak shifts (0.1–0.2 meV) are large relative to the superconducting gap magnitude of UTe_2 (~0.25 meV), which is difficult to reconcile with a phase-gradient effect. We therefore conclude that the phase/superfluid effect, while possibly present as a subdominant contribution, is not the primary origin of the observed spectral evolution.

Another important finding of this work is that when the Yang vortex overlaps with the step edge, the ZECP originally present in the free Yang vortex is locally suppressed. Microscopically, this suppression may originate either from a modification of the underlying zero-energy state itself or from an interaction-induced redistribution of the local spectral weight between the vortex and step-edge states; our present data cannot unambiguously distinguish between these possibilities. In previous studies [39–41], this ZECP has been proposed as a candidate signature of MZMs. If further confirmed, our observation suggests that this spectroscopic signature may be locally tuned by step edges. We further demonstrate that vortices in UTe_2 can be manipulated by the STM tip (Supplementary Note 8 of SM), consistent with the relatively weak vortex pinning in this system [39,41,50]. This tip-induced vortex motion provides an additional route—in addition to magnetic field tuning—for positioning vortices with respect to step edges. The combination of magnetic field, STM tip manipulation, and engineered step-edge geometries thus opens up the possibility of achieving spatially selective control of candidate MZMs, a key step toward their potential application in topological quantum devices.

In summary, our work reveals the position-dependent interaction between step-edge states and Yin-Yang vortex states on the UTe_2 (011) surface, and shows that the step edges can locally tune vortex zero modes. These findings not only deepen our understanding of the interplay among TSS, boundary states, and vortex bound states in UTe_2, but also provide new perspectives for the manipulation of candidate MZMs and the design of topological quantum devices. Furthermore, our results impose important constraints on theoretical models: what pairing symmetry and topological boundary states can give rise to such coupling effects? These questions await further investigations.

Data availability

The main data supporting the findings of this study are available within the article and its SM. All the raw data generated in this study are available from the corresponding author upon request.

Acknowledgments

This work was supported by the Quantum Science and Technology-National Science and Technology Major Project [Grant No. 2021ZD0302803 (D.L.F.)], the HFNL Self-Deployed Project [ZB2602000301 (Y.J.Y.)], the National Key R&D Program of the MOST of China [Grant No. 2023YFA1406304 (Y.J.Y.)], the National Natural Science Foundation of China [Grant Nos. 12374140 (Y.J.Y.), U23A20580 (S.Y.T.), and 12494593 (Y.J.Y.)], the New Cornerstone Science Foundation (D.L.F.), the Sichuan Science and Technology Program [Grant No. 2025NSFJQ0040 (S.Y.T.)], and the Anhui Provincial Natural Science Foundation (Grant No. 2508085J001).

References

[1] Leggett A J 1975 *Rev. Mod. Phys.* **47** 331
[2] Sigrist M and Ueda K 1991 *Rev. Mod. Phys.* **63** 239
[3] Huy N T, Gasparini A, De Nijs D E, Huang Y, Klaasse J C P, Gortenmulder T, De Visser A, Hamann A, Görlach T, and Löhneysen H V 2007 *Phys. Rev. Lett.* **99** 067006
[4] Aoki D, Ishida K, and Flouquet J 2019 *J. Phys. Soc. Jpn.* **88** 022001
[5] Mineev V P 2017 *Phys. -Usp.* **60** 121
[6] Lévy F, Sheikin I, Grenier B, and Huxley A D 2005 *Science* **309** 1343
[7] Sato M and Ando Y 2017 *Rep. Prog. Phys.* **80** 076501
[8] Sato M 2009 *Phys. Rev. B* **79** 214526
[9] Tanaka Y, Sato M, and Nagaosa N 2012 *J. Phys. Soc. Jpn.* **81** 011013
[10] Salomaa M M and Volovik G E 1985 *Phys. Rev. Lett.* **55** 1184
[11] Autti S, Dmitriev V V, Mäkinen J T, Soldatov A A, Volovik G E, Yudin A N, Zavjalov V V, and Eltsov V B 2016 *Phys. Rev. Lett.* **117** 255301
[12] Read N and Green D 2000 *Phys. Rev. B* **61** 10267
[13] Ivanov D A 2001 *Phys. Rev. Lett.* **86** 268
[14] Qi X L and Zhang S C 2011 *Rev. Mod. Phys.* **83** 1057
[15] Alicea J 2012 *Rep. Prog. Phys.* **75** 076501
[16] Ran S, Eckberg C, Ding Q P, Furukawa Y, Metz T, Saha S R, Liu I L, Zic M, Kim H, Paglione J, and Butch N P 2019 *Science* **365** 684
[17] Aoki D, Nakamura A, Honda F, Li D, Homma Y, Shimizu Y, Sato Y J, Knebel G, Brison J P, Pourret A, Braithwaite D, Lapertot G, Niu Q, Vališka M, Harima H, and Flouquet J 2019 *J. Phys. Soc. Jpn.* **88** 043702
[18] Fujibayashi H, Nakamine G, Kinjo K, Kitagawa S, Ishida K, Tokunaga Y, Sakai H, Kambe S, Nakamura A, Shimizu Y, Homma Y, Li D, Honda F, and Aoki D 2022 *J. Phys. Soc. Jpn.* **91** 043705
[19] Metz T, Bae S, Ran S, Liu I L, Eo Y S, Fuhrman W T, Agterberg D F, Anlage S M, Butch N P, and Paglione J 2019 *Phys. Rev. B* **100** 220504
[20] Kittaka S, Shimizu Y, Sakakibara T, Nakamura A, Li D, Homma Y, Honda F, Aoki D, and Machida K 2020 *Phys. Rev. Research* **2** 032014
[21] Jiao L, Howard S, Ran S, Wang Z, Rodriguez J O, Sigrist M, Wang Z, Butch N P, and Madhavan V 2020 *Nature* **579** 523
[22] Bae S, Kim H, Eo Y S, Ran S, Liu I, Fuhrman W T, Paglione J, Butch N P, and Anlage S M 2021 *Nat. Commun.* **12** 2644
[23] Hayes I M, Wei D S, Metz T, Zhang J, Eo Y S, Ran S, Saha S R, Collini J, Butch N P, Agterberg D F, Kapitulnik A, and Paglione J 2021 *Science* **373** 797
[24] Gu Q, Wang S, Carroll J P, Zhussupbekov K, Broyles C, Ran S, Butch

N P, Horn J A, Saha S, Paglione J, Liu X, Davis J C S, and Lee D H 2025 *Science* **388** 938
[25] Li Z, Moir C M, McKee N J, Lee-Wong E, Baumbach R E, Maple M B, and Liu Y 2025 *Proc. Natl. Acad. Sci. U. S. A.* **122** e2419734122
[26] Wang S, Zhussupbekov K, Carroll J P, Hu B, Liu X, Pangburn E, Crepieux A, Pepin C, Broyles C, Ran S, Butch N P, Saha S, Paglione J, Bena C, Davis J C S, and Gu Q 2025 *Nat. Phys.* **21** 1555
[27] Matsumura H, Takahashi Y, Matsubayashi R, Kinjo K, Kitagawa S, Ishida K, Tokunaga Y, Sakai H, Kambe S, Kimata M, Nakamura A, Shimizu Y, Homma Y, Li D, Honda F, Miyake A, Aoki D, Furukawa T, and Sasaki T 2026 *Phys. Rev. B* **113** 094506
[28] Totsuka K, Kono Y, Shimizu Y, Nakamura A, Miyake A, Aoki D, Tsutsumi Y, Machida K, and Kittaka S 2026 *J. Phys. Soc. Jpn.* **95** 034709
[29] Nakamine G, Kinjo K, Kitagawa S, Ishida K, Tokunaga Y, Sakai H, Kambe S, Nakamura A, Shimizu Y, Homma Y, Li D, Honda F, and Aoki D 2021 *Phys. Rev. B* **103** L100503
[30] Matsumura H, Fujibayashi H, Kinjo K, Kitagawa S, Ishida K, Tokunaga Y, Sakai H, Kambe S, Nakamura A, Shimizu Y, Homma Y, Li D, Honda F, and Aoki D 2023 *J. Phys. Soc. Jpn.* **92** 063701
[31] Matsumura H, Takahashi Y, Kinjo K, Kitagawa S, Ishida K, Tokunaga Y, Sakai H, Kambe S, Nakamura A, Shimizu Y, Homma Y, Li D, Honda F, Miyake A, and Aoki D 2025 *Phys. Rev. B* **111** 174526
[32] Nakamine G, Kitagawa S, Ishida K, Tokunaga Y, Sakai H, Kambe S, Nakamura A, Shimizu Y, Homma Y, Li D, Honda F, and Aoki D 2019 *J. Phys. Soc. Jpn.* **88** 113703
[33] Rosuel A, Marcenat C, Knebel G, Klein T, Pourret A, Marquardt N, Niu Q, Rousseau S, Demuer A, Seyfarth G, Lapertot G, Aoki D, Braithwaite D, Flouquet J, and Brison J P 2023 *Phys. Rev. X* **13** 011022
[34] Ran S, Liu I L, Eo Y S, Campbell D J, Neves P M, Fuhrman W T, Saha S R, Eckberg C, Kim H, Graf D, Balakirev F, Singleton J, Paglione J, and Butch N P 2019 *Nat. Phys.* **15** 1250
[35] Knebel G, Knafo W, Pourret A, Niu Q, Vališka M, Braithwaite D, Lapertot G, Nardone M, Zitouni A, Mishra S, Sheikin I, Seyfarth G, Brison J P, Aoki D, and Flouquet J 2019 *J. Phys. Soc. Jpn.* **88** 063707
[36] Braithwaite D, Vališka M, Knebel G, Lapertot G, Brison J P, Pourret A, Zhitomirsky M E, Flouquet J, Honda F, and Aoki D 2019 *Commun. Phys.* **2** 147
[37] Aoki D, Honda F, Knebel G, Braithwaite D, Nakamura A, Li D, Homma Y, Shimizu Y, Sato Y J, Brison J P, and Flouquet J 2020 *J. Phys. Soc. Jpn.* **89** 053705
[38] Wu Z, Weinberger T I, Chen J, Cabala A, Chichinadze D V, Shaffer D, Pospíšil J, Prokleška J, Haidamak T, Bastien G, Sechovský V, Hickey A J, Mancera-Ugarte M J, Benjamin S, Graf D E, Skourski Y, Lonzarich G G, Vališka M, Grosche F M, and Eaton A G 2024 *Proc. Natl. Acad. Sci. U. S. A.* **121** e2403067121
[39] Yin R, Li Y, Du Z, Yuan D, Wang S, Gong J, Li M, Chen Z, Zhang J, Wang Y, Xue Z, Lai X, Tan S, Wang D, Wang Q H, Feng D L, and Yan Y J 2026 *Nat. Commun.* **17** 5394
[40] Sharma N, Toole M, McKenzie J, Cheng F, Bordelon M M, Thomas S M, Rosa P F S, Hsu Y T, and Liu X 2025 *ACS Nano* **19** 31539
[41] Yang Z, Zheng F, Wu D, Zhang B B, Li N, Li W, Zhang C, Zhang G M, Chen X, Chen Y, and Yan S 2025 *Natl. Sci. Rev.* **12** nwaf267
[42] Azari N, Yakovlev M, Rye N, Dunsiger S R, Sundar S, Bordelon M M, Thomas S M, Thompson J D, Rosa P F S, and Sonier J E 2023 *Phys. Rev. Lett.* **131** 226504
[43] Ajeesh M O, Bordelon M, Girod C, Mishra S, Ronning F, Bauer E D, Maiorov B, Thompson J D, Rosa P F S, and Thomas S M 2023 *Phys. Rev. X* **13** 041019
[44] Yu Y, Madhavan V, and Raghu S 2022 *Phys. Rev. B* **105** 174520
[45] Yokoyama T, Iniotakis C, Tanaka Y, and Sigrist M 2008 *Phys. Rev. Lett.* **100** 177002
[46] Yoshida S, Suzuki S I, and Tanaka Y 2022 *Phys. Rev. Research* **4** 043122
[47] Fogelström M, Rainer D, and Sauls J A 1997 *Phys. Rev. Lett.* **79** 281
[48] Aprili M, Badica E, and Greene L H 1999 *Phys. Rev. Lett.* **83** 4630
[49] Graser S, Iniotakis C, Dahm T, and Schopohl N 2004 *Phys. Rev. Lett.* **93** 247001
[50] Tokiwa Y, Sakai H, Kambe S, Opletal P, Yamamoto E, Kimata M, Awaji S, Sasaki T, Yanase Y, Haga Y, and Tokunaga Y 2023 *Phys. Rev. B* **108** 144502